# Fundamental Limitations for DOA Estimation by a Sphere

Nordebo, Sven; Gustafsson, Mats

2004

CODEN:LUTEDX/(TEAT-7128)/1-26/(2004)

# Fundamental Limitations for DOA Estimation by a Sphere

**Sven Nordebo and Mats Gustafsson**

Department of Electroscience
Electromagnetic Theory
Lund Institute of Technology
Sweden

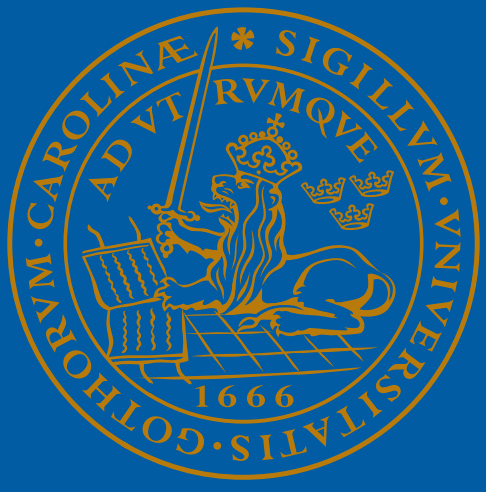

Sven Nordebo

School of Mathematics and System Engineering
Växjö University
Växjö
Sweden

Mats Gustafsson

Department of Electroscience
Electromagnetic Theory
Lund Institute of Technology
P.O. Box 118
SE-221 00 Lund
Sweden

Editor: Gerhard Kristensson

**Abstract**

In this paper we consider fundamental limitations for DOA estimation with arbitrary lossless antennas or antenna arrays inserted inside a sphere. Spherical vector modes and their associated equivalent circuits and Q factor approximations are employed as a general framework for the analysis. The classical broadband matching theory by Fano is extended to a general multiport S–parameter model of the antennas and fundamental bounds are given for the scattering parameters with respect to bandwidth and electrical size of the sphere. Finally, assuming a statistical signal model with Gaussian receiver noise, the Cramer–Rao lower bound is used to derive fundamental upper bounds for the performance of DOA estimation by a sphere.

# 1 Introduction

The Direction of Arrival (DOA) estimation using antenna arrays has been the topic for research in array and statistical signal processing over several decades and comprises now well developed modern techniques such as maximum likelihood and subspace methods, see e.g. [12, 18, 22] and the references therein. Statistical, and parametric estimation methods for sensor arrays typically rely on certain geometrical properties of the assumed propagation model such as known *steering vectors* or *array manifold* together with a statistical signal model for the receiver noise. Efficient, modern parametric estimation methods then result in a resolution capability which is not limited by the array aperture, provided that the data collection time or SNR are sufficiently large and assuming that the data model accurately reflects the experimental scenario [12]. Recently, there has been an increased interest in incorporating properties of electromagnetic wave propagation with the statistical signal estimation techniques used for sensor array processing and there are several papers dealing with direction finding using electromagnetic vector sensors and diversely polarized antenna arrays, tripole arrays, etc., see e.g. [10, 14, 15, 19, 23, 24].

In many cases it is desired to design systems that both have a high estimation performance and a small physical size. Unfortunately, the antenna performance deteriorates when the antenna gets electrically small. The drawback of small antennas as being narrowband and lossy are well known [2, 8], and the same will of course be true for an array of antennas confined within a given volyme. In this paper we analyze in detail how the fundamental physical limitations of antennas have implications on the performance of DOA estimation with arbitrary lossless antennas or antenna arrays inserted inside a sphere. In particular, we are interested in the optimum estimation performance implied by the electrical size of the antennas as well as the bandwidth of the system.

To analyze the estimation performance of a volume, it is essential to relate three classical theories giving fundamental limitations in the disciplines estimation theory, antenna theory and broadband matching. Assuming a Gaussian signal model for the receiver noise, the Cramer–Rao bound [11] can be used as a performance measure for the estimation. The classical theory of radiating Q uses spherical vector

modes and equivalent circuits to analyze the properties of a hypothetical antenna inside a sphere, c.f. [2, 3, 6–9, 16, 20]. An antenna with a high Q factor has electromagnetic fields with large amounts of stored energy around it, and hence, typically low bandwidth and high losses [8]. The mode expansion also gives a natural expression of the polarization, angle and spatial diversity that is utilized with array processing systems. The classical theory of broadband matching shows how much power that can be transmitted between a transmission line and a given load [5], i.e. the antenna. In this paper we show that the classical broadband matching theory by Fano can be extended to a general multiport S–parameter model of an antenna array and fundamental bounds are given for the scattering parameters with respect to bandwidth and electrical size of the sphere. Assuming a statistical signal model with Gaussian receiver noise, the Cramer–Rao lower bound is then used to obtain fundamental upper bounds for the performance of DOA estimation by a sphere.

The paper is outlined as follows. An introduction is given in section 1. In section 2 is given a detailed signal model for a receiving antenna array. We start by defining a multiport S–parameter model for transmitting antenna arrays and then use the reciprocity theorem to develop a multiport model for receiving arrays. The section is concluded by incorporating a statistical signal model including Gaussian receiver noise, and fundamental lower bounds are given for the accuracy of DOA estimation with respect to the scattering parameters. Section 3 contains the Fano broadband matching theory for the multiport S–parameter model with explicit results for the first order spherical vector modes as well as for the general Q factor approximations. Section 4 contains a number of numerical examples regarding fundamental DOA estimation properties with respect to electrical size of the antennas and bandwidth of the system.

# 2 Signal model for receiving antennas

## 2.1 A multiport scattering model for transmitting antennas

In order to develop a general signal model for receiving antennas we start by considering the electromagnetic fields associated with arbitrary antennas in the transmit mode, and then apply the reciprocity theorem to obtain the properties of the corresponding antennas in the receive mode.

We consider the electromagnetic field which is propagated into free space when the transmitting antennas (all sources) are contained inside a sphere of radius $r = a$. Let $k = \omega/c$ denote the wave number, $\omega = 2\pi f$ the frequency, and $c$ and $\eta$ the speed of light and the wave impedance of free space, respectively. The transmitted electric and magnetic fields, $\boldsymbol{E}(\boldsymbol{r})$ and $\boldsymbol{H}(\boldsymbol{r})$, can then be expanded in *outgoing spherical*

*vector waves* $\boldsymbol{u}_{\tau ml}(k\boldsymbol{r})$ as [9]

$$\boldsymbol{E}(\boldsymbol{r}) = \sum_{l=1}^{\infty}\sum_{m=-l}^{l}\sum_{\tau=1}^{2} f_{\tau ml}\boldsymbol{u}_{\tau ml}(k\boldsymbol{r}) \tag{2.1}$$

$$\boldsymbol{H}(\boldsymbol{r}) = -\frac{1}{\mathrm{i}\eta}\sum_{l=1}^{\infty}\sum_{m=-l}^{l}\sum_{\tau=1}^{2} f_{\tau ml}\boldsymbol{u}_{\bar{\tau} ml}(k\boldsymbol{r}) \tag{2.2}$$

where $f_{\tau ml}$ are the expansion coefficients or multipole moments and $\bar{\tau}$ denotes the complementary index. Here $\tau = 1$ ($\bar{\tau} = 2$) corresponds to a transversal electric (TE) wave and $\tau = 2$ ($\bar{\tau} = 1$) corresponds to a transversal magnetic (TM) wave. The other indices are $l = 1, 2, \ldots, \infty$ and $m = -l \ldots, l$ where $l$ denotes the *order* of that mode.

It can be shown that in the *far field* when $r \to \infty$, the electric field is given by

$$\boldsymbol{E}(\boldsymbol{r}) = \frac{\mathrm{e}^{-\mathrm{i}kr}}{kr}\boldsymbol{F}(\hat{\boldsymbol{r}}) \tag{2.3}$$

where $\boldsymbol{F}(\hat{\boldsymbol{r}})$ is the *far field amplitude* given by

$$\boldsymbol{F}(\hat{\boldsymbol{r}}) = \sum_{l=1}^{\infty}\sum_{m=-l}^{l}\sum_{\tau=1}^{2} \mathrm{i}^{l+2-\tau} f_{\tau ml}\boldsymbol{A}_{\tau ml}(\hat{\boldsymbol{r}}) \tag{2.4}$$

and $\boldsymbol{A}_{\tau ml}(\hat{\boldsymbol{r}})$ denotes the *spherical vector harmonics* [9]. Furthermore, it can also be shown that the total power $P_s$ transmitted by the antenna can be expressed in terms of the expansion coefficients as

$$P_s = \frac{1}{2\eta k^2}\sum_{l=1}^{\infty}\sum_{m=-l}^{l}\sum_{\tau=1}^{2} |f_{\tau ml}|^2. \tag{2.5}$$

For further details about the spherical vector mode representation we refer to Appendix A and [9, 13].

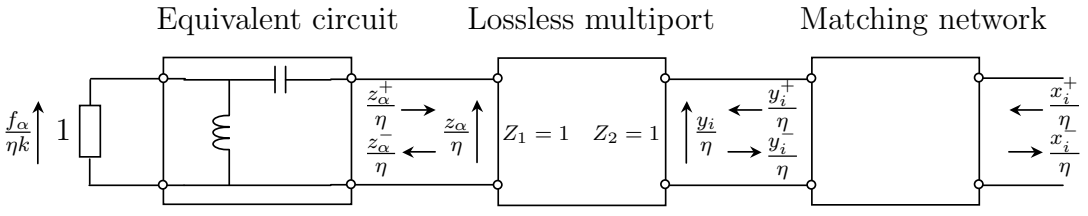


**Figure 1**: Normalized multiport model of a lossless antenna.

Next, we assume that the antenna is lossless and can be modeled using a normalized multiport as shown in Fig. 1 where a finite number of modes $M$ is employed. As was originally described by Chu in [2], an arbitrary antenna inside a sphere of

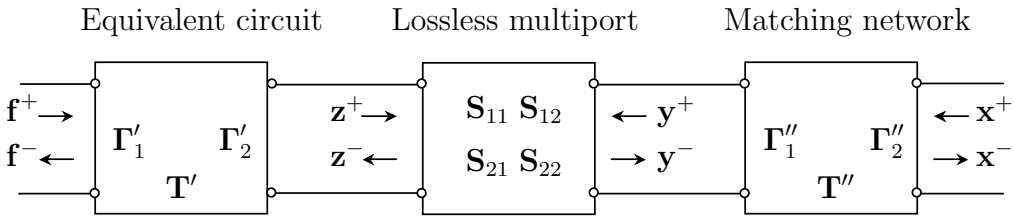


**Figure 2**: Normalized multiport model of a lossless antenna, matrix form. The reflection and transmission matrices $\boldsymbol{\Gamma}$ and $\mathbf{T}$ are diagonal and the scattering matrix $\mathbf{S}$ is general (lossless and reciprocal).

radius $a$ can be modeled using a coupling network connecting independent equivalent circuits representing each spherical mode. The propagated power for each mode is represented by the power loss over the terminating resistance $\eta$ and the wave impedance as seen by the spherical mode at radius $a$ is equal to the input impedance of the equivalent circuit for all frequencies. In Appendix A we derive the four possible equivalent circuits for TE and TM modes of even and odd order and an electric circuit analogy for the terminal quantities.

In Fig. 1, $x_i^+$ and $x_i^-$ denote the incident and reflected voltages at the antenna waveguide connections for $i = 1, \ldots, N$ where $N$ is the number of antenna ports. These voltages are normalized so that the power delivered to a particular antenna port is $\frac{|x_i^+|^2}{2\eta}$ and the corresponding reflected power is $\frac{|x_i^-|^2}{2\eta}$. For simplicity, we assume that the transmission line characteristic impedance is the same as the wave impedance $\eta$ of free space. Each antenna port may be connected to a lossless matching network in which case $y_i^+$ and $y_i^-$ denote the wave amplitudes at the antenna waveguide connections as depicted in Fig. 1.

In the left end of Fig. 1, we let the voltage $\frac{f_\alpha}{\eta k}$ represent the propagated wave amplitude where $f_\alpha$ denotes the expansion coefficients for the spherical vector waves as in (2.1). Here, the multi–index $\alpha = (l, m, \tau)$ is chosen to simplify the notation. The multiport model of Fig. 1 is normalized to the wave impedance $\eta$ and the totally transmitted power for each mode is thus equal to $\frac{1}{2\eta k^2}|f_\alpha|^2$ as in (2.5).

The total voltage at each antenna port is denoted $y_i$, and the normalized voltage at the input of the TE or TM equivalent circuit is defined by

$$\frac{z_\alpha}{\eta} = \frac{f_\alpha}{\eta k}\frac{V_n}{V_0} \tag{2.6}$$

where $V_n$ and $V_0$ are defined as in (A.11) in Appendix A.

It is assumed that the relation between incident and reflected wave quantities in Fig. 1 can be represented by a scattering matrix as

$$\begin{pmatrix} \mathbf{z}^- \\ \mathbf{y}^- \end{pmatrix} = \begin{pmatrix} \mathbf{S}_{11} & \mathbf{S}_{12} \\ \mathbf{S}_{21} & \mathbf{S}_{22} \end{pmatrix} \begin{pmatrix} \mathbf{z}^+ \\ \mathbf{y}^+ \end{pmatrix} = \mathbf{S} \begin{pmatrix} \mathbf{z}^+ \\ \mathbf{y}^+ \end{pmatrix} \tag{2.7}$$

where the dimension of the matrices $\mathbf{S}_{11}$, $\mathbf{S}_{12}$, $\mathbf{S}_{21}$ and $\mathbf{S}_{22}$ are $M \times M$, $M \times N$,

$N \times M$ and $N \times N$, respectively. The matrix $\mathbf{S}$ is assumed to be lossless ($\mathbf{S}^{\mathrm{H}}\mathbf{S} = \mathbf{I}$) and reciprocal ($\mathbf{S} = \mathbf{S}^{\mathrm{T}}$).

In the normalized model of Fig. 1, all port resistances are 1 Ohm. The matrix form for the normalized multiport model is depicted in Fig. 2. We have the following scattering parameters

$$\begin{pmatrix} \mathbf{f}^- \\ \mathbf{z}^+ \end{pmatrix} = \begin{pmatrix} \mathbf{\Gamma}'_1 & \mathbf{T}' \\ \mathbf{T}' & \mathbf{\Gamma}'_2 \end{pmatrix} \begin{pmatrix} \mathbf{f}^+ \\ \mathbf{z}^- \end{pmatrix} \tag{2.8}$$

and

$$\begin{pmatrix} \mathbf{y}^+ \\ \mathbf{x}^- \end{pmatrix} = \begin{pmatrix} \mathbf{\Gamma}''_1 & \mathbf{T}'' \\ \mathbf{T}'' & \mathbf{\Gamma}''_2 \end{pmatrix} \begin{pmatrix} \mathbf{y}^- \\ \mathbf{x}^+ \end{pmatrix} \tag{2.9}$$

where all reflection and transmission matrices $\mathbf{\Gamma}$ and $\mathbf{T}$ are diagonal.

By solving (2.7) through (2.9) for $\mathbf{f}^-$ and $\mathbf{x}^-$ when $\mathbf{f}^+$ and $\mathbf{x}^+$ are given, we get the total scattering matrix

$$\begin{pmatrix} \mathbf{f}^- \\ \mathbf{x}^- \end{pmatrix} = \begin{pmatrix} \bar{\mathbf{S}}_{11} & \bar{\mathbf{S}}_{12} \\ \bar{\mathbf{S}}_{21} & \bar{\mathbf{S}}_{22} \end{pmatrix} \begin{pmatrix} \mathbf{f}^+ \\ \mathbf{x}^+ \end{pmatrix} = \bar{\mathbf{S}} \begin{pmatrix} \mathbf{f}^+ \\ \mathbf{x}^+ \end{pmatrix} \tag{2.10}$$

where

$$\bar{\mathbf{S}}_{11} = \mathbf{\Gamma}'_1 + \mathbf{T}'\mathbf{K}^{-1}\left(\mathbf{S}_{11} + \mathbf{S}_{12}\mathbf{\Gamma}''_1\mathbf{M}^{-1}\mathbf{S}_{21}\right)\mathbf{T}' \tag{2.11}$$

$$\bar{\mathbf{S}}_{12} = \mathbf{T}'\mathbf{K}^{-1}\mathbf{S}_{12}\left(\mathbf{I} + \mathbf{\Gamma}''_1\mathbf{M}^{-1}\mathbf{S}_{22}\right)\mathbf{T}'' \tag{2.12}$$

$$\tag{2.13}$$

and

$$\mathbf{K} = \mathbf{I} - \mathbf{S}_{11}\mathbf{\Gamma}'_2 - \mathbf{S}_{12}\mathbf{\Gamma}''_1\mathbf{M}^{-1}\mathbf{S}_{21}\mathbf{\Gamma}'_2 \tag{2.14}$$

$$\mathbf{M} = \mathbf{I} - \mathbf{S}_{22}\mathbf{\Gamma}''_1. \tag{2.15}$$

Since the antenna is assumed to be lossless and reciprocal we have $\bar{\mathbf{S}}^{\mathrm{H}}\bar{\mathbf{S}} = \mathbf{I}$ and $\bar{\mathbf{S}}^{\mathrm{T}} = \bar{\mathbf{S}}$ implying that $\bar{\mathbf{S}}_{11}^{\mathrm{H}}\bar{\mathbf{S}}_{11} + \bar{\mathbf{S}}_{21}^{\mathrm{H}}\bar{\mathbf{S}}_{21} = \mathbf{I}$ and $\bar{\mathbf{S}}_{21}^{\mathrm{T}} = \bar{\mathbf{S}}_{12}$.

We note that the normalized multiport model described above can be interpreted as a vector two–port model which generalizes the well known result for $M = N = 1$, $\mathbf{S}_{11} = \mathbf{S}_{22} = 0$, $\mathbf{S}_{21} = \mathbf{S}_{12} = 1$, and hence

$$\bar{S}_{11} = \Gamma'_1 + \frac{T'^2\Gamma''_1}{1 - \Gamma''_1\Gamma'_2} \tag{2.16}$$

$$\bar{S}_{12} = \frac{T'T''}{1 - \Gamma''_1\Gamma'_2} \tag{2.17}$$

cf. e.g. [5]. Here $|\bar{S}_{11}|^2 + |\bar{S}_{21}|^2 = 1$ and $\bar{S}_{21} = \bar{S}_{12}$.

As an idealized mode–coupled antenna we assume that $M = N$, $\mathbf{S}_{11} = \mathbf{S}_{22} = \mathbf{0}$, and that $\mathbf{S}_{21}$ and $\mathbf{S}_{12}$ are diagonal. Since $\mathbf{S}$ is reciprocal ($\mathbf{S}^{\mathrm{T}} = \mathbf{S}$) we have $\mathbf{S}_{12} = \mathbf{S}_{21}^{\mathrm{T}} = \mathbf{S}_{21}$. Since $\mathbf{S}$ is lossless ($\mathbf{S}^{\mathrm{H}}\mathbf{S} = \mathbf{I}$) we have that $\mathbf{S}_{12}^{\mathrm{H}}\mathbf{S}_{12} = \mathbf{I}$, and we conclude that the diagonal elements of $\mathbf{S}_{12}$ have unit magnitude.

The scattering parameters of (2.10) become

$$\bar{\mathbf{S}}_{11} = \boldsymbol{\Gamma}_1' + \mathbf{S}_{12}^2 \mathbf{T}'^2 \mathbf{K}^{-1} \boldsymbol{\Gamma}_1'' \tag{2.18}$$
$$\bar{\mathbf{S}}_{12} = \mathbf{S}_{12} \mathbf{T}' \mathbf{T}'' \mathbf{K}^{-1} \tag{2.19}$$
$$\tag{2.20}$$

and

$$\mathbf{K} = \mathbf{I} - \mathbf{S}_{12}^2 \boldsymbol{\Gamma}_1'' \boldsymbol{\Gamma}_2' \tag{2.21}$$

where all matrices are diagonal.

## 2.2 Multiport scattering model for receiving antennas

Next, we derive the multiport scattering model for receiving antennas by considering the reciprocity theorem. On transmission the transmitted wave field is given by $\mathbf{f}^- = \bar{\mathbf{S}}_{12}\mathbf{x}^+$. Thus, if we consider the transmitted wave field $f_\alpha$ due to one single input terminal with the incident voltage wave $x_i^+$, we get the output $f_\alpha = k \left[\bar{\mathbf{S}}_{12}\right]_{\alpha,i} x_i^+$. Now, from the antenna reciprocity theorem [4] we have

$$x_i^- x_i^+ = -\mathrm{i}\frac{\lambda^2}{2\pi} \boldsymbol{F}(\hat{\boldsymbol{k}}_0) \cdot \boldsymbol{E}_0 \tag{2.22}$$

where $\boldsymbol{E}_0$ is the complex vector amplitude of an incoming plane wave $\boldsymbol{E}_0 \mathrm{e}^{-\mathrm{i}k\hat{\boldsymbol{k}}_0 \cdot \boldsymbol{r}}$ from direction $\hat{\boldsymbol{k}}_0$ and $x_i^-$ the corresponding received signal. Further, $\boldsymbol{F}(\hat{\boldsymbol{r}})$ is the far field amplitude corresponding to the transmitted signal $x_i^+$. Hence, by using (2.4) the received signal is obtained from the reciprocity theorem (2.22) as

$$\mathbf{x}^- = \frac{2\pi}{k} \bar{\mathbf{S}}_{21} \mathbf{A} \mathbf{E} \tag{2.23}$$

where $\mathbf{A}$ is an $M \times 2$ matrix where each row corresponds to the spherical components of the spherical vector harmonics $\mathrm{i}^{l+1-\tau} \boldsymbol{A}_\alpha(\hat{\boldsymbol{k}}_0)$, and $\mathbf{E}$ is an $2 \times 1$ vector containing the corresponding signal components of the electric field $\boldsymbol{E}_0$.

## 2.3 Statistical signal model and accuracy bounds for DOA estimation

In this section we employ a simple statistical signal model in order to derive accuracy bounds for the estimation of Direction Of Arrival (DOA) parameters, with regard to the scattering parameters previously described.

The received signal in (2.23) is in principal given in the frequency domain. However, we will consider a signal snapshot model [21] where time domain samples are taken in the baseband. We consider a situation where the received electric field is monochromatic and completely polarized. We assume a narrowband signal model where $k$ corresponds to the carrier frequency $\omega_0$ and the *fractional bandwidth* $B = \frac{\Delta\omega}{\omega_0}$ is reasonable low. Here $\Delta\omega$ denotes the absolute bandwidth. It is further assumed

that the receiver baseband noise are Nyquist samples of a white complex Gaussian stochastic process [17] which has been filtered through an ideal lowpass filter with bandwidth $\Delta\omega$. Thus, the discrete time sensor noise is white complex Gaussian with a variance $\sigma_n^2$ which is assumed to be proportional to the bandwidth, $\sigma_n^2 = N_0\omega_0 B$ where $N_0$ is the spectral density of the Gaussian process.

Now, from (2.23) the received signal is given by

$$\mathbf{x}(t) = \frac{2\pi}{k}\bar{\mathbf{S}}_{21}\mathbf{A}\mathbf{E} + \mathbf{n}(t) \tag{2.24}$$

where $\mathbf{n}(t)$ is white complex Gaussian noise with covariance matrix $\sigma_n^2\mathbf{I}$. The received signal $\mathbf{x}(t)$ is therefore complex Gaussian with mean

$$\boldsymbol{\mu} = \mathcal{E}\left\{\mathbf{x}(t)\right\} = \frac{2\pi}{k}\bar{\mathbf{S}}_{21}\mathbf{A}\mathbf{E} \tag{2.25}$$

and covariance matrix

$$\mathbf{C} = \mathcal{E}\left\{(\mathbf{x}(t) - \boldsymbol{\mu})(\mathbf{x}(t) - \boldsymbol{\mu})^{\mathrm{H}}\right\} = \sigma_n^2\mathbf{I} \tag{2.26}$$

where $\mathcal{E}\left\{\cdot\right\}$ denotes the expectation operator.

We are interested in the estimation accuracy of the spherical DOA parameters $\theta$ and $\phi$ which we write as a vector parameter $\boldsymbol{\xi} = [\theta\ \phi]^{\mathrm{T}}$. For the complex Gaussian case, the *Fisher information matrix* is generally given by [11]

$$[\mathbf{I}(\boldsymbol{\xi})]_{ij} = \mathrm{tr}\left\{\mathbf{C}^{-1}\frac{\partial\mathbf{C}}{\partial\xi_i}\mathbf{C}^{-1}\frac{\partial\mathbf{C}}{\partial\xi_j}\right\} + 2\,\mathrm{Re}\left\{\frac{\partial\boldsymbol{\mu}^{\mathrm{H}}}{\partial\xi_i}\mathbf{C}^{-1}\frac{\partial\boldsymbol{\mu}}{\partial\xi_j}\right\} \tag{2.27}$$

which becomes in our particular case

$$[\mathbf{I}(\boldsymbol{\xi})]_{ij} = \frac{8\pi^2}{\sigma_n^2 k^2}\,\mathrm{Re}\left\{\mathbf{p}_i^{\mathrm{H}}\bar{\mathbf{S}}_{21}^{\mathrm{H}}\bar{\mathbf{S}}_{21}\mathbf{p}_j\right\} \tag{2.28}$$

where

$$\mathbf{p}_i = \frac{\partial}{\partial\xi_i}\left\{\mathbf{A}\mathbf{E}\right\}. \tag{2.29}$$

Now, the Cramer–Rao lower bound (CRLB) for estimating the parameter $\xi_i$ is given by [11]

$$\mathrm{var}\left\{\hat{\xi}_i\right\} \geq \left[\mathbf{I}^{-1}(\boldsymbol{\xi})\right]_{ii} \geq \frac{1}{[\mathbf{I}(\boldsymbol{\xi})]_{ii}} \tag{2.30}$$

where

$$[\mathbf{I}(\boldsymbol{\xi})]_{ii} = \frac{8\pi^2}{\sigma_n^2 k^2}\mathbf{p}_i^{\mathrm{H}}\bar{\mathbf{S}}_{21}^{\mathrm{H}}\bar{\mathbf{S}}_{21}\mathbf{p}_i \tag{2.31}$$

which is real and nonnegative. Since $\bar{\mathbf{S}}$ is lossless we have $\bar{\mathbf{S}}_{21}^{\mathrm{H}}\bar{\mathbf{S}}_{21} + \bar{\mathbf{S}}_{11}^{\mathrm{H}}\bar{\mathbf{S}}_{11} = \mathbf{I}$ and the eigenvalues of $\bar{\mathbf{S}}_{21}^{\mathrm{H}}\bar{\mathbf{S}}_{21}$ are in the interval $[0, 1]$. It is therefore concluded that

$$[\mathbf{I}(\boldsymbol{\xi})]_{ii} \leq \frac{8\pi^2}{\sigma_n^2 k^2}\mathbf{p}_i^{\mathrm{H}}\mathbf{p}_i. \tag{2.32}$$

Hence, a lower bound for var $\left\{\hat{\xi}_i\right\}$ is given by

$$\text{var}\left\{\hat{\xi}_i\right\} \geq \frac{1}{[\mathbf{I}(\boldsymbol{\xi})]_{ii}} \geq \frac{k^2 N_0 \omega_0}{8\pi^2} F_{\text{a}} \tag{2.33}$$

where we have defined

$$F_{\text{a}} = \frac{B}{\mathbf{p}_i^{\text{H}} \mathbf{p}_i} \tag{2.34}$$

as the *accuracy factor* which depends on bandwidth, but is independent of matching. It is observed that the accuracy bound of (2.33) and the accuracy factor of (2.34) do not necessarily give the greatest lower bound for var $\left\{\hat{\xi}_i\right\}$. However, the resulting bounds are valid for general antennas and can be used to investigate the estimation performance with respect to bandwidth and optimum matching of the reflection coefficients $\Gamma_j$.

We note also that for the idealized mode–coupled antenna where $\bar{\mathbf{S}}_{11}$ is diagonal, the CRLB expression (2.31) can be calculated when the reflection coefficients $|\Gamma_j|^2$ are known

$$[\mathbf{I}(\boldsymbol{\xi})]_{ii} = \frac{8\pi^2}{\sigma_n^2 k^2} \mathbf{p}_i^{\text{H}} \left(\mathbf{I} - \bar{\mathbf{S}}_{11}^{\text{H}} \bar{\mathbf{S}}_{11}\right) \mathbf{p}_i. \tag{2.35}$$

The final bound for var $\left\{\hat{\xi}_i\right\}$ in (2.30) becomes

$$\text{var}\left\{\hat{\xi}_i\right\} \geq \frac{1}{[\mathbf{I}(\boldsymbol{\xi})]_{ii}} = \frac{k^2 N_0 \omega_0}{8\pi^2} F_{\text{a}}^{\text{CRLB}} \tag{2.36}$$

where

$$F_{\text{a}}^{\text{CRLB}} = \frac{B}{\mathbf{p}_i^{\text{H}} \text{diag}\left[1 - |\Gamma_j|^2\right] \mathbf{p}_i} \tag{2.37}$$

is an accuracy factor directly related to the Cramer–Rao lower bound. Here, we use the notion diag $[1 - |\Gamma_j|^2]$ for the diagonal matrix with diagonal elements $1 - |\Gamma_j|^2$.

## 2.4 Explicit expressions for the Cramer–Rao lower bound

As an example of an explicit derivation of the Cramer–Rao bound we consider the estimation of the polar angle $\theta$ when $\theta = 0$, using an idealized mode–coupled antenna as described above and a linear polarization $\boldsymbol{E}_0 = E_0 \hat{\boldsymbol{\theta}}$ of the incoming field. We have for the denominator in (2.37)

$$\mathbf{p}_i^{\text{H}} \text{diag}\left[1 - |\Gamma_j|^2\right] \mathbf{p}_i = |E_0|^2 \sum_{l=1}^{\infty} \sum_{m=-l}^{l} \frac{1 - |\Gamma_{ml}|^2}{l(l+1)} \left( \left| \frac{\partial}{\partial \theta} \frac{1}{\sin\theta} \frac{\partial \text{Y}_{ml}}{\partial \phi} \right|^2 + \left| \frac{\partial^2 \text{Y}_{ml}}{\partial \theta^2} \right|^2 \right) \tag{2.38}$$

where $\text{Y}_{ml}$ are the spherical harmonics given by

$$\text{Y}_{ml}(\theta, \phi) = \sqrt{\frac{2l+1}{4\pi}} \sqrt{\frac{(l-m)!}{(l+m)!}} \text{P}_l^m(\cos\theta) \text{e}^{\text{i}m\phi} \tag{2.39}$$

and where $\mathrm{P}_l^m(x)$ are the associated Legendre functions, cf. [9, 13]. Using recursive relations for the associated Legendre functions we have

$$\frac{\partial^2}{\partial\theta^2}\mathrm{P}_l^m(\cos\theta)|_{\theta=0} = \frac{1}{4}\delta_{m+2} - \frac{1}{2}l(l+1)\delta_m + \frac{1}{4}(l-1)l(l+1)(l+2)\delta_{m-2} \tag{2.40}$$

and we can calculate

$$\sum_{lm}\frac{1-|\Gamma_{ml}|^2}{l(l+1)}\left|\frac{\partial^2\mathrm{Y}_{ml}}{\partial\theta^2}\right|^2_{\theta=0} = \sum_{l=1}^{\infty}\left(1-|\Gamma_l|^2\right)\frac{2l+1}{32\pi}\left(3l^2+3l-2\right). \tag{2.41}$$

Furthermore, by using the definition of the associated Legendre functions generated via the Legendre polynomials $\mathrm{P}_l(x)$, we find the relation

$$\frac{\partial}{\partial\theta}\frac{1}{\sin\theta}\mathrm{P}_l^m(\cos\theta)|_{\theta=0} = \mathrm{P}_l''|_{x=1}\left(\delta_{m-2} + \frac{(l-2)!}{(l+2)!}\delta_{m+2}\right) \tag{2.42}$$

where

$$\mathrm{P}_l''|_{x=1} = \frac{(l-1)l(l+1)(l+2)}{8} \tag{2.43}$$

and we can calculate

$$\sum_{lm}\frac{1-|\Gamma_{ml}|^2}{l(l+1)}\left|\frac{\partial}{\partial\theta}\frac{1}{\sin\theta}\frac{\partial\mathrm{Y}_{ml}}{\partial\phi}\right|^2_{\theta=0} = \sum_{l=2}^{\infty}\left(1-|\Gamma_l|^2\right)\frac{2l+1}{32\pi}\left(l^2+l-2\right). \tag{2.44}$$

We get finally

$$\mathbf{p}_i^{\mathrm{H}}\mathrm{diag}\left[1-|\Gamma_j|^2\right]\mathbf{p}_i = |E_0|^2\sum_{l=1}^{\infty}\left(1-|\Gamma_l|^2\right)\frac{2l+1}{8\pi}\left(l^2+l-1\right). \tag{2.45}$$

# 3 Broadband Fano theory for the multiport model

In this section we show that some of the important theoretical limitations for two–port broadband matching of arbitrary impedances as given by Fano in [5], can be generalized to the multiport model described previously in section 2.1.

As a starting point we consider the scattering matrix $\bar{\mathbf{S}}_{11}$ given in (2.11) and assume that the diagonal elements $T_j'$ of the transmission coefficient $\mathbf{T}'$ has a *common* zero at $s=0$ with multiplicity $n$. Denote the diagonal elements of $\bar{\mathbf{S}}_{11}$ by $\Gamma_j$ and the elements of $\mathbf{\Gamma}_1'$ by $\Gamma_j'$. The Taylor series expansion of the logarithm of the diagonal elements $\Gamma_j$ about $s=0$ can then be written

$$\log\frac{1}{\Gamma_j} = A_1 s + \cdots + A_{2k+1}s^{2k+1} + \cdots + A_{2n-1}s^{2n-1} + \cdots \tag{3.1}$$

where even order coefficients up to and including $2n-2$ are zero, and the odd coefficients $A_{2k+1}$ are independent of the matching network ($\mathbf{\Gamma}_1''$, $\mathbf{\Gamma}_2''$, $\mathbf{T}''$) for $k = 0, 1, \ldots, n-1$.

These facts are now established as follows. Since $s = 0$ is a common zero of $\mathbf{T}'$ of multiplicity $n$, it follows from (2.11) that

$$\frac{d^k}{s^k}\Gamma_j = \frac{d^k}{s^k}\Gamma'_j \tag{3.2}$$

for $s = 0$ and $k = 0, 1, \ldots, 2n-1$. Hence, the Taylor coefficients $A_k$ for $\log \frac{1}{\Gamma_j}$ and $\log \frac{1}{\Gamma'_j}$ are equal for $k = 0, 1, \ldots, 2n-1$. The Taylor coefficient $A_0 = 0$ since $\Gamma_j(0) = \Gamma'_j(0)$ and we assume that $\Gamma'_j(0) = 1$. Furthermore, we have the relation $|\Gamma'_j(\mathrm{i}\omega)|^2 + |T'_j(\mathrm{i}\omega)|^2 = 1$ and since $|T'_j(\mathrm{i}\omega)|^2$ has a zero of multiplicity $2n$ at $\omega = 0$ we have

$$\frac{d^k}{d\omega^k} \log |\Gamma'_j(\mathrm{i}\omega)| = \frac{d^k}{d\omega^k} |\Gamma'_j(\mathrm{i}\omega)|^2 = 0 \tag{3.3}$$

for $\omega = 0$ and $k = 1, \ldots, 2n-1$. Hence, since $\log |\Gamma_j(\mathrm{i}\omega)|$ is an even function, the corresponding even coefficients $A_k$ in (3.1) are zero up to and including $2n-2$.

Now, assume that the reflection coefficient $\Gamma_j$ has zeros $s_{oi}$ and poles $s_{pi}$ so that

$$\log \frac{1}{\Gamma_j} = \sum \log(s - s_{pi}) - \sum \log(s - s_{oi}) \tag{3.4}$$

it is then readily verified that the Taylor coefficients of (3.1) are given by

$$A_{2k+1} = \frac{1}{2k+1} \left( \sum s_{oi}^{-2k-1} - \sum s_{pi}^{-2k-1} \right) \tag{3.5}$$

which are invariant to the choice of $\Gamma_j$ or $\Gamma'_j$ for $k = 0, 1, \ldots, n-1$. The prerequisites are now identical to the development in [5], and by employing the calculus of residues the following integral relation is obtained

$$\int_0^\infty \frac{1}{\omega^{2(k+1)}} \log \frac{1}{|\Gamma_j|} \, \mathrm{d}\omega = (-1)^k \frac{\pi}{2} \frac{1}{2k+1} \left[ \sum s_{oi}^{-2k-1} - \sum s_{pi}^{-2k-1} - 2 \sum s_{ri}^{-2k-1} \right] \tag{3.6}$$

for $k = 0, 1, \ldots, n-1$ and where $s_{ri}$ are the zeros of $\Gamma_j$ in the right half–plane. When calculating the residues above it is observed that it is necessary that even order Taylor coefficients vanish up to and including $2n-2$. Note that the first two sums on the right hand side of (3.6) are proportional to $A_{2k+1}$ in (3.5) and can therefore be computed from the zeros $s'_{oi}$ and poles $s'_{pi}$ of $\Gamma'_j$.

If the diagonal elements $T'_j$ of $\mathbf{T}'$ has a common zero at infinity $s = \infty$ with multiplicity $n$, the previous result can be readily employed by the substitution $z = s^{-1}$. The resulting integral relation is

$$\int_0^\infty \omega^{2k} \log \frac{1}{|\Gamma_j|} \, \mathrm{d}\omega = (-1)^k \frac{\pi}{2} \frac{1}{2k+1} \left[ \sum s_{oi}^{2k+1} - \sum s_{pi}^{2k+1} - 2 \sum s_{ri}^{2k+1} \right] \tag{3.7}$$

for $k = 0, 1 \ldots, n-1$.

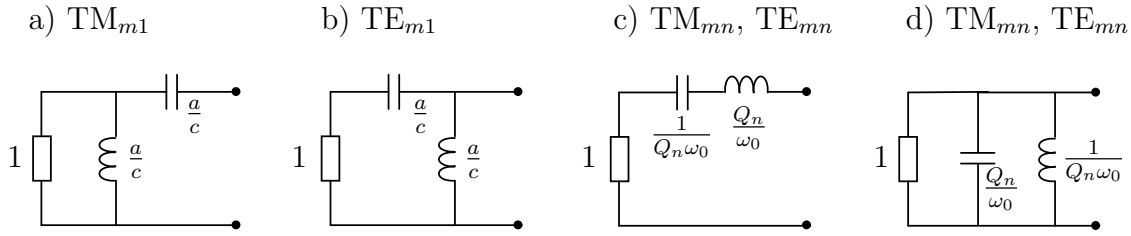


**Figure 3**: Circuit models of spherical modes. The resistor models the radiation part. The capacitor and inductor model the parts that stores the electric field and magnetic field, respectively. Figures a) and b) are exact circuit equivalents for the TM$_{m1}$ and TE$_{m1}$ modes, respectively. Figures c) and d) are series and parallel RCL Q–factor approximations, respectively, which are valid for general TM$_{mn}$ or TE$_{mn}$modes.

## 3.1 Fundamental bounds for the lowest order modes

The transmission coefficients $T_j'$ for all modes with equivalent circuits depicted in Fig. 13 have a double zero ($n = 2$) at $s = 0$. The first six modes of order $n = 1$ consists of a ladder circuit containing one capacitance $a/c$ and one inductance $a/c$ and a 1 Ohm terminating resistance, cf. Figs. 3 a) and b).

The transmission coefficients are given by

$$T_j'(s) = \frac{2s^2(\frac{a}{c})^2}{2s^2(\frac{a}{c})^2 + 2s\frac{a}{c} + 1} \tag{3.8}$$

with a double zero at $s = 0$, and the reflection coefficients are

$$\Gamma_j'(s) = \frac{1}{2s^2(\frac{a}{c})^2 + 2s\frac{a}{c} + 1} \tag{3.9}$$

with no zeros and poles $s_{pi}' = \frac{c}{2a}(-1 \pm \mathrm{i})$ and ${s_{pi}'}^{-1} = \frac{a}{c}(-1 \pm \mathrm{i})$.

By assuming a constant reflection coefficient $|\Gamma_j|$ over the bandwidth $[\omega_0 - \omega_0\frac{B}{2}, \omega_0 + \omega_0\frac{B}{2}]$ and introducing the constant $K = \frac{2}{\pi}\log\frac{1}{|\Gamma_j|}$, the two integrals of (3.6) for $k = 0, 1$ become

$$K\frac{B}{1 - B^2/4} = 2ka - 2\sum\frac{\omega_0}{s_{ri}} \tag{3.10}$$

$$K\frac{B + B^3/12}{(1 - B^2/4)^3} = \frac{4}{3}(ka)^3 + \frac{2}{3}\sum\left(\frac{\omega_0}{s_{ri}}\right)^3. \tag{3.11}$$

Since $\mathrm{Re}\left\{\frac{\omega_0}{s_{ri}}\right\} > 0$, the relation (3.10) implies the inequality $|\Gamma_j| \geq \mathrm{e}^{-\pi ka\frac{(1-B^2/4)}{B}}$. However, this is not a greatest lower bound and cannot be achieved. Instead we aim to solve (3.10) and (3.11) for $B$ fixed.

Since $\mathrm{Re}\left\{\frac{\omega_0}{s_{ri}}\right\} > 0$, we have

$$\mathrm{Re}\left\{\left(\frac{\omega_0}{s_{ri}}\right)^3\right\} < \left(\mathrm{Re}\left\{\frac{\omega_0}{s_{ri}}\right\}\right)^3 \tag{3.12}$$

and thus,

$$\sum \mathrm{Re}\left\{\left(\frac{\omega_0}{s_{ri}}\right)^3\right\} < \sum\left(\mathrm{Re}\left\{\frac{\omega_0}{s_{ri}}\right\}\right)^3 \leq \left(\sum \mathrm{Re}\left\{\frac{\omega_0}{s_{ri}}\right\}\right)^3. \tag{3.13}$$

We wish to minimize the right hand side of (3.13) and at the same time to maximize the left hand side. The optimum solution is thus obtained by employing one single real term in (3.13), $x = \frac{\omega_0}{s_{ri}}$. The equations (3.10) and (3.11) become

$$K\frac{B}{1-B^2/4} = 2ka - 2x \tag{3.14}$$

$$K\frac{B+B^3/12}{(1-B^2/4)^3} = \frac{4}{3}(ka)^3 + \frac{2}{3}x^3 \tag{3.15}$$

which is a nonlinear system of equations in the unknowns $K$ and $x$, and which can be solved by using numerical methods. We will refer to the corresponding solution $|\Gamma_j| = \mathrm{e}^{-\frac{\pi}{2}K}$ as the Fano limit.

It is also possible to derive a narrowband approximation based on (3.14) and (3.15) as follows. We get for $B \ll 1$

$$KB \leq 2ka - 2x \tag{3.16}$$

$$KB \leq \frac{4}{3}(ka)^3 + \frac{2}{3}x^3. \tag{3.17}$$

Combining these inequalities, we get

$$KB \leq \frac{4}{3}(ka)^3 + \frac{2}{3}(ka - \frac{1}{2}KB)^3 = 2(ka)^3 - (ka)^2 KB + \frac{1}{2}kaK^2B^2 - \frac{1}{12}K^3B^3 \leq 2(ka)^3 \tag{3.18}$$

when $B \ll 1$. The narrowband approximation is hence given by

$$|\Gamma_j| \geq \mathrm{e}^{-\frac{\pi}{B}(ka)^3}. \tag{3.19}$$

## 3.2 Fundamental bounds for the Q-factor approximation

In theory, the equivalent circuits can be used to derive a Fano limit for any TE or TM mode. However, this is rather tedious due to the complex structure of these higher order modes together with the nonlinearity of the Fano theory. Moreover, it is known that it is advantageous to mix the TE and TM modes in high bandwidth systems [9]. Instead of using the analytic expressions of the impedance it is common to use the Q–factor (quality factor, antenna Q or radiation Q) to get an estimate of the bandwidth. Since there is an extensive literature on the Q–factor for antennas, see e.g. [2, 3, 6–9, 16, 20], only some of the results are given here. The Q of the antenna is defined as the quotient between the power stored in the reactive fields and the radiated power [2, 9]

$$Q = \frac{2\omega \max(W_{\mathrm{M}}, W_{\mathrm{E}})}{P} \tag{3.20}$$

where $\omega$ is the angular frequency, $W_{\mathrm{M}}$ stored magnetic energy, $W_{\mathrm{E}}$ stored electric energy, and $P$ the dissipated power. At the resonance frequency of the antenna, there are equal amounts of stored electric energy and stored magnetic energy, i.e. $W_{\mathrm{E}} = W_{\mathrm{M}}$. The Q–factor is related to the bandwidth of the corresponding resonance circuit as $\Delta f/f_0 \approx Q^{-1}$ for $Q \gg 1$. The Q–factor can either be determined by the equivalent circuits [2, 9] or by an analytic expression involving spherical Hankel functions [3]. The six lowest order modes have $Q = (ka)^{-1}+(ka)^{-3}$. By combination of one $TE_{m1}$ mode and one $TM_{m1}$ mode the Q–factor is reduced to $Q = (ka)^{-1} + (ka)^{-3}/2$.

At and around the resonance frequency, $\omega_0 = 2\pi f_0$, the antenna model is given by a resonance circuit. The impedance of the antenna is only matched to the feeding network at the resonance frequency. The resonance circuit is either a series RCL circuit with capacitance $\frac{1}{Q\omega_0}$ and inductance $\frac{Q}{\omega_0}$, or a parallel circuit with these values switched. Again, the resonance circuit is terminated with a 1 Ohm resistance modeling the propagated power, cf. Figs. 3 c) and d).

The transmission coefficients for the Q–factor resonance circuits are given by

$$T_j'(s) = \frac{\frac{2}{Q}\frac{s}{\omega_0}}{1 + \frac{2}{Q}\frac{s}{\omega_0} + (\frac{s}{\omega_0})^2} \tag{3.21}$$

with one single zero at $s = 0$ and one single zero at $s = \infty$. Note that these zeros are common for all modes. The reflection coefficients are

$$\Gamma_j'(s) = \frac{1 + (\frac{s}{\omega_0})^2}{1 + \frac{2}{Q}\frac{s}{\omega_0} + (\frac{s}{\omega_0})^2} \tag{3.22}$$

with zeros at $s'_{oi} = \pm \mathrm{i}\omega_0$ and poles $s'_{pi} = \frac{\omega_0}{Q}(-1 \pm \mathrm{i}\sqrt{Q^2-1})$ and ${s'_{pi}}^{-1} = \frac{1}{\omega_0 Q}(-1 \pm \mathrm{i}\sqrt{Q^2-1})$.

By assuming a constant reflection coefficient $|\Gamma_j|$ over the bandwidth $[\omega_0 - \omega_0\frac{B}{2}, \omega_0 + \omega_0\frac{B}{2}]$ and introducing the constant $K = \frac{2}{\pi}\log\frac{1}{|\Gamma_j|}$, the two integrals of (3.6) and (3.7) for $k = 0$ become

$$\frac{KB}{1 - B^2/4} = \frac{2}{Q} - 2\sum\frac{\omega_0}{s_{ri}} \tag{3.23}$$

$$KB = \frac{2}{Q} - 2\sum\frac{s_{ri}}{\omega_0}. \tag{3.24}$$

We can see that these equations can be satisfied by one complex conjugated pair $s_{ri}$ and $s_{ri}^*$ as follows. Let $\frac{s_{ri}}{\omega_0} = x + \mathrm{i}y$, then $\mathrm{Re}\left\{\frac{s_{ri}}{\omega_0}\right\} = x$ and $\mathrm{Re}\left\{\frac{\omega_0}{s_{ri}}\right\} = \frac{x}{x^2+y^2}$. Since $KB < KB/(1 - B^2/4)$, the equations can be satisfied by letting $y \to \infty$ and then chosing a suitable $x > 0$. Hence, the relation (3.23) gives an inequality which is a greatest lower bound for $|\Gamma_j|$

$$|\Gamma_j| \geq e^{-\frac{\pi}{Q}\frac{1-B^2/4}{B}}. \tag{3.25}$$

We will refer to this bound as the Q–factor approximation.

# 4 Numerical Examples

Next, we give a number of numerical examples to highlight the properties of the fundamental bounds derived for DOA estimation. We start by studying general properties of optimum Fano–matching with respect to bandwidth $B$ and electrical size $ka$, as well as the behavior of the accuracy factor $F_{\mathrm{a}}$ which is valid for arbitrary antennas. We also compare the general results to the Cramer–Rao lower bound accuracy factor $F_{\mathrm{a}}^{\mathrm{CRLB}}$ which is explicitly derived for some interesting special cases.

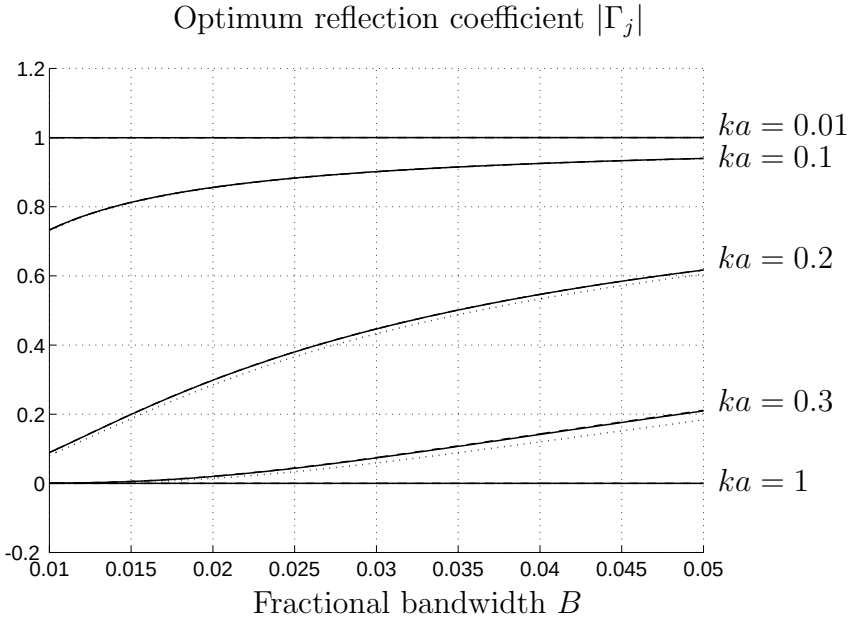


**Figure 4**: Optimum reflection coefficient $|\Gamma_j|$ for the $n = 1$ modes as a function of fractional bandwidth $B$ and various values of $ka$. Solid line: Fano limit. Dashed line (coinciding with solid line): Q-factor approximation. Dotted line: Narrowband approximation.

## 4.1 Fundamental limitations for general antennas

In Fig. 4 is shown the optimum reflection coefficient $|\Gamma_j|$ for the $n = 1$ modes as a function of fractional bandwidth $B$ and various values of $ka$. The solid line is the Fano limit defined by (3.14) and (3.15). The dashed line (coinciding with the solid line) is the Q-factor approximation defined in (3.25) with $Q = (ka)^{-1} + (ka)^{-3}$. Thus, the Q–factor yield a very good approximation (indistinguishable plots) for the Fano limit for the $n = 1$ modes. The dotted line is the narrowband approximation defined in (3.19). This is a good approximation for the Fano limit in narrowband cases when $B \ll 1$, however as is expected, we can see that it is not the greatest lower bound for $|\Gamma_j|$.

In Fig. 5 is shown the optimum reflection coefficient $|\Gamma_j|$ for the first 3 mode orders $n = 1, 2, 3$ as a function of fractional bandwidth $B$ when $ka = \frac{1}{2}$. The

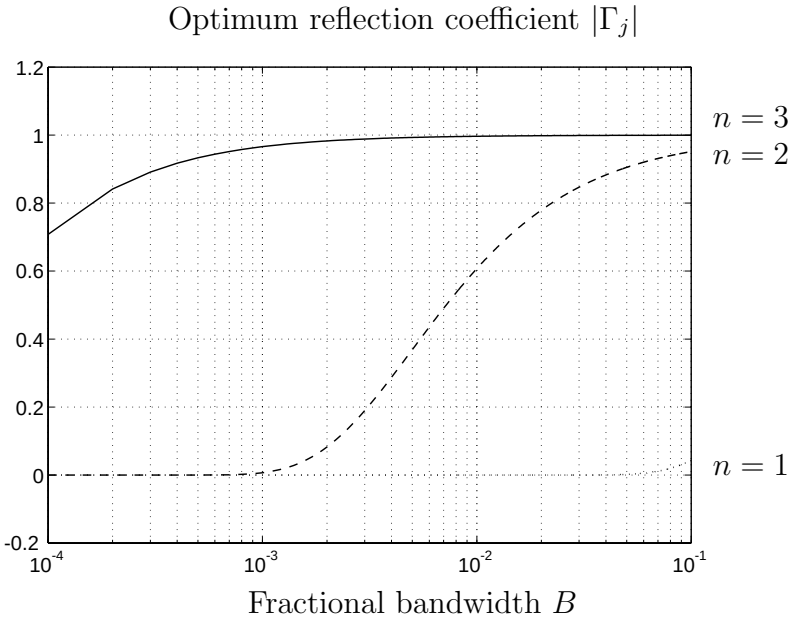


**Figure 5**: Optimum reflection coefficient $|\Gamma_j|$ for the first 3 mode orders $n = 1, 2, 3$ as a function of fractional bandwidth $B$. Electrical size is $ka = \frac{1}{2}$. Solid line: $n = 3$. Dashed line: $n = 2$. Dotted line: $n = 1$.

reflection coefficients are calculated according to the Q–factor approximation given in (3.25) with

$$Q_1 = \frac{1}{ka} + \frac{1}{(ka)^3} \tag{4.1}$$

$$Q_2 = \frac{3}{ka} + \frac{6}{(ka)^3} + \frac{18}{(ka)^5} \tag{4.2}$$

$$Q_3 = \frac{6}{ka} + \frac{21}{(ka)^3} + \frac{135}{(ka)^5} + \frac{675}{(ka)^7} \tag{4.3}$$

for the first 3 mode orders, cf. [3]. The plot illustrates the fact that for a given electrical size $ka$, all modes will ultimately be useless (useful), i.e. $|\Gamma|$ will approach unity (zero) as the bandwidth $B$ increases (decreases). Furthermore, for a given bandwidth $B$, there is always a certain limited number of modes that are useful with $|\Gamma|$ significantly less than unity.

In Fig. 6 is shown the accuracy factor $F_{\mathrm{a}}$ for DOA estimation given in (2.34) for the first 3 mode orders $n = 1, 2, 3$, as a function of fractional bandwidth $B$ when $ka = \frac{1}{2}$. In Fig. 6 is also shown the Cramer–Rao lower bound accuracy factor $F_{\mathrm{a}}^{\mathrm{CRLB}}$ given in (2.37) for the explicit case derived in section 2.4 and (2.45), together with the Q–factors $Q_1$, $Q_2$ and $Q_3$ as given above. The solid line shows three mode orders included $n = 1, 2, 3$ ($M = 30$), the dashed line shows two mode orders included $n = 1, 2$ ($M = 16$), and the dotted line show one mode order included $n = 1$ ($M = 6$). This example illustrates the fact that as the bandwidth increases, the accuracy of DOA estimation is determined by a decreasing number of modes. In this example with $ka = \frac{1}{2}$, it is sufficient to consider 3 mode orders for the lower

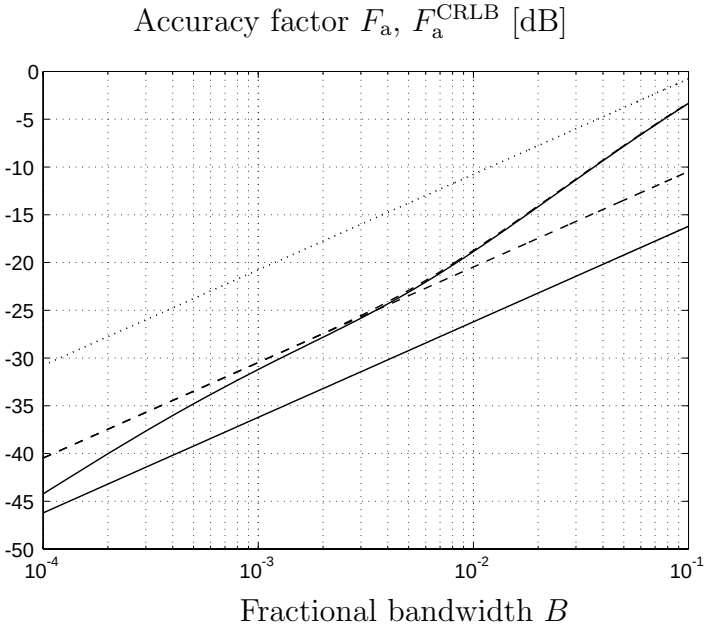


**Figure 6**: Accuracy factor $F_{\rm a}$ and $F_{\rm a}^{\rm CRLB}$ for the first 3 mode orders $n = 1, 2, 3$ as a function of fractional bandwidth $B$. Electrical size is $ka = \frac{1}{2}$. Solid line: Three mode orders included $n = 1, 2, 3$. Dashed line: Two mode orders included $n = 1, 2$. Dotted line: One mode order included $n = 1$.

bandwidths and 2 mode orders for the higher bandwidths. This figure should be compared to the optimum reflection coefficients of Fig. 5.

In Fig. 7 is shown the optimum reflection coefficient $|\Gamma_j|$ for the first 3 mode orders $n = 1, 2, 3$, as a function of the electrical size $ka$ when $B = 0.01$. The reflection coefficients are calculated according to the Q–factor approximation given in (3.25) with $Q_1$, $Q_2$ and $Q_3$ as given above. The plot illustrates the fact that for a given bandwidth $B$, all modes will ultimately be useless (useful), i.e. $|\Gamma|$ will approach unity (zero) as the electrical size $ka$ decreases (increases). Furthermore, for a given electrical size $ka$, there is always a certain limited number of modes that are useful with $|\Gamma|$ significantly less than unity.

In Fig. 8 is shown the accuracy factors $F_{\rm a}$ and $F_{\rm a}^{\rm CRLB}$ in the same example as above, but here as a function of the electrical size $ka$ when $B = 0.01$. The solid line shows three mode orders included $n = 1, 2, 3$, the dashed line shows two mode orders included $n = 1, 2$, and the dotted line show one mode order included $n = 1$. This example illustrates the fact that as the electrical size $ka$ decreases, the accuracy of DOA estimation is determined by a decreasing number of modes. In this example with $B = 0.01$, it is sufficient to consider 3 mode orders for $ka = 1$, 2 mode orders for $ka = 0.5$ and 1 mode order for $ka = 0.1$. This figure should be compared to the optimum reflection coefficients of Fig. 7.

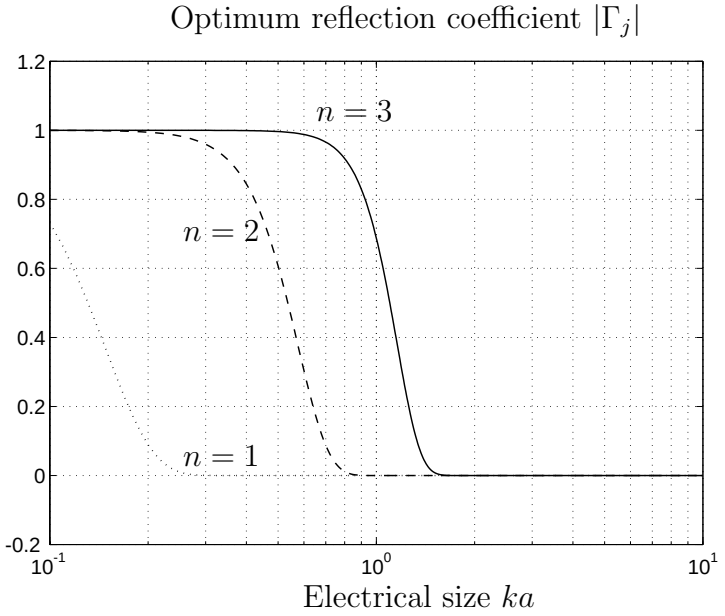


**Figure 7**: Optimum reflection coefficient $|\Gamma_j|$ for the first 3 mode orders $n = 1, 2, 3$ as a function of electrical size $ka$. Fractional bandwidth is $B = 0.01$. Solid line: $n = 3$. Dashed line: $n = 2$. Dotted line: $n = 1$.

## 4.2 Fundamental limitations for the idealized mode–coupled antenna

Next, we study the DOA estimation performance of the idealized mode–coupled antenna. We consider the Cramer–Rao lower bound accuracy factor $F_{\mathrm{a}}^{\mathrm{CRLB}}$ given in (2.37) together with the Q–factor approximation in (3.25) and Q–factors (4.1) through (4.3). We consider the case of estimating the azimuthal spherical angle $\phi$ when the angle $\theta$ is given. Further, we assume that the polarization is linear with $\boldsymbol{E}_0 = E_0 \cdot \hat{\boldsymbol{\theta}}$. Hence, in (2.37) we have used

$$\mathbf{p}_i^{\mathrm{H}} \mathrm{diag}\left[1 - |\Gamma_j|^2\right] \mathbf{p}_i = |E_0|^2 \sum_{ml} \frac{1 - |\Gamma_{ml}|^2}{l(l+1)} \left[ \left| \frac{1}{\sin\theta} \frac{\partial^2}{\partial\phi^2} \mathrm{Y}_{ml} \right|^2 + \left| \frac{\partial^2}{\partial\phi\partial\theta} \mathrm{Y}_{ml} \right|^2 \right] \quad (4.4)$$

where $|\Gamma_{ml}|$ is the optimum reflection coefficient calculated using (3.25).

In Fig. 9 is shown the Cramer–Rao lower bound accuracy factor $F_{\mathrm{a}}^{\mathrm{CRLB}}$ for the first 3 mode orders $n = 1, 2, 3$ as a function of the spherical angle $\theta$. Here the fractional bandwidth is $B = 0.01$ and the electrical size $ka = \frac{1}{2}$ or $ka = \infty$. The solid line shows three mode orders included $n = 1, 2, 3$ ($M = 30$), the dashed line shows two mode orders included $n = 1, 2$ ($M = 16$), and the dotted line show one mode order included $n = 1$ ($M = 6$). In this example, there is a significant gain in going from one mode order ($n = 1$) to two mode orders ($n = 1, 2$) included. However, the inclusion of a third mode order ($n = 1, 2, 3$) does not contribute much when $ka = \frac{1}{2}$. The figure also illustrates the possible gain of using two or three mode orders when $ka$ is large enough ($ka = \infty$). Qualitatively, we will of course see the same effect also for higher order modes, i.e. for a given electrical size and bandwidth

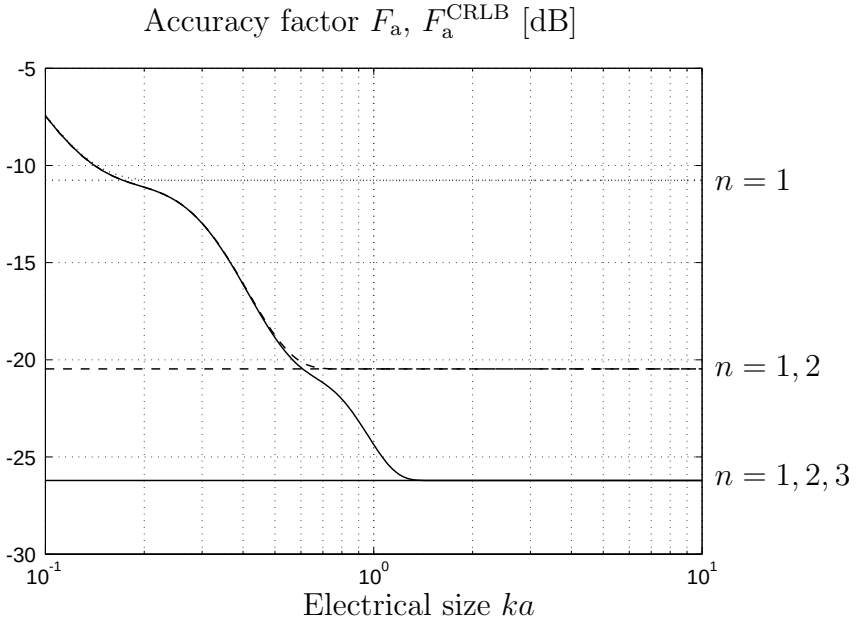


**Figure 8**: Accuracy factor $F_{\mathrm{a}}$ and $F_{\mathrm{a}}^{\mathrm{CRLB}}$ for the first 3 mode orders $n = 1, 2, 3$ as a function of electrical size $ka$. Fractional bandwidth is $B = 0.01$. Solid line: Three mode orders included $n = 1, 2, 3$. Dashed line: Two mode orders included $n = 1, 2$. Dotted line: One mode order included $n = 1$.

there will always be a limited number of modes that contribute to the Cramer–Rao lower bound.

In this example, it is noted that the Cramer–Rao lower bound is independent of the azimuthal angle $\phi$, but is dependent on the elevation angle $\theta$ as indicated in Fig. 9. This may seem odd at first since we expect the estimation performance of a sphere to be spherically symmetrical, i.e. independent of the DOA. However, it should be noted that as soon as the coordinate system has been fixed, the spherical modes have properties that are not spherically symmetrical, cf. [1]. In this case this means simply that the optimum performance for estimating $\phi$ when $\theta$ is known is obtained by chosing a new coordinate system such that $\theta = \pi/2$, c.f. Fig. 9.

In Fig. 10 is shown the Cramer–Rao lower bound accuracy factor $F_{\mathrm{a}}^{\mathrm{CRLB}}$ for the first 3 mode orders $n = 1, 2, 3$ as a function of fractional bandwidth $B$. Here $\theta = \pi/2$ and $ka = \frac{1}{2}$. The solid line shows three mode orders included $n = 1, 2, 3$ ($M = 30$), the dashed line shows two mode orders included $n = 1, 2$ ($M = 16$), and the dotted line show one mode order included $n = 1$ ($M = 6$). This figure should be compared to the optimum reflection coefficients of Fig. 5 and the behavior of the general accuracy factor of Fig. 6.

In Fig. 11 is shown the Cramer–Rao lower bound accuracy factor $F_{\mathrm{a}}^{\mathrm{CRLB}}$ for the first 3 mode orders $n = 1, 2, 3$ as a function of electrical size $ka$. Here $\theta = \pi/2$ and $B = 0.01$. The solid line shows three mode orders included $n = 1, 2, 3$, the dashed line shows two mode orders included $n = 1, 2$, and the dotted line show one mode order included $n = 1$. This figure should be compared to the optimum reflection coefficients of Fig. 7 and the behavior of the general accuracy factor of Fig. 8.

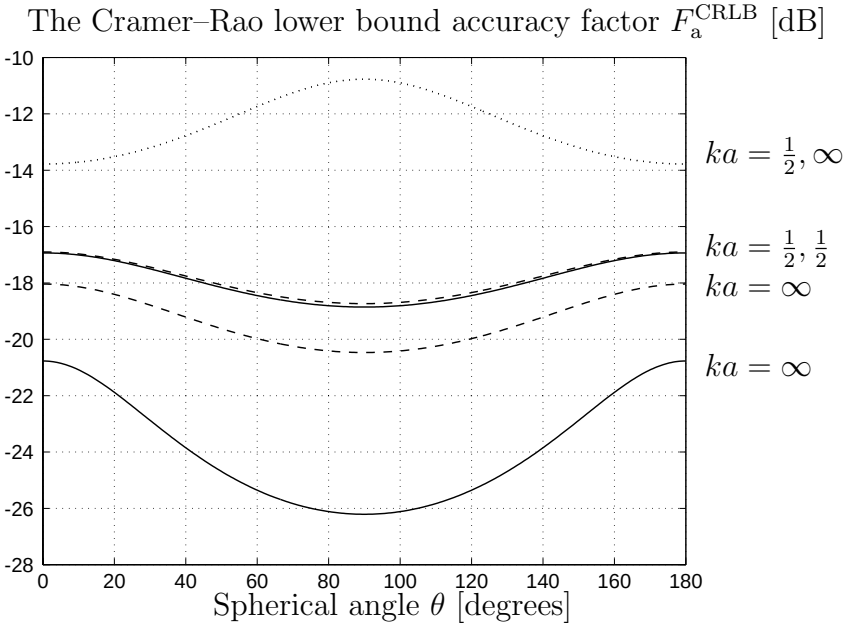


**Figure 9**: The Cramer–Rao lower bound accuracy factor $F_{\mathrm{a}}^{\mathrm{CRLB}}$ for the first 3 mode orders $n = 1, 2, 3$ as a function of the spherical angle $\theta$. Here the fractional bandwidth is $B = 0.01$ and the electrical size $ka = \frac{1}{2}$ or $ka = \infty$. Solid line: Three mode orders included $n = 1, 2, 3$. Dashed line: Two mode orders included $n = 1, 2$. Dotted line: One mode order included $n = 1$.

# 5 Summary

To analyze the estimation performance of a volume, it is essential to relate three classical theories giving fundamental limitations in the disciplines estimation theory, antenna theory and broadband matching. In this paper we consider fundamental limitations for DOA estimation with arbitrary lossless antennas or antenna arrays inserted inside a sphere.

A signal model for receiving antenna arrays is developed by defining a multiport scattering S–parameter model for transmitting antennas and then using the reciprocity theorem to obtain a multiport model for receiving antennas. A statistical signal model including Gaussian receiver noise is adopted and fundamental lower bounds are given for the accuracy of DOA estimation with respect to the scattering parameters of this model. Classical antenna theory with spherical vector modes and their associated equivalent circuits and Q factor approximations are employed as a general framework for the analysis. We show that the classical broadband matching theory by Fano can be extended to the general multiport S–parameter model of the antenna array and fundamental bounds are given for the scattering parameters with respect to bandwidth and electrical size of the sphere. Explicit results for the first order spherical vector modes as well as for the general Q factor approximations are given.

Finally, a number of numerical examples are given regarding fundamental DOA estimation properties with respect to electrical size of the antennas and bandwidth

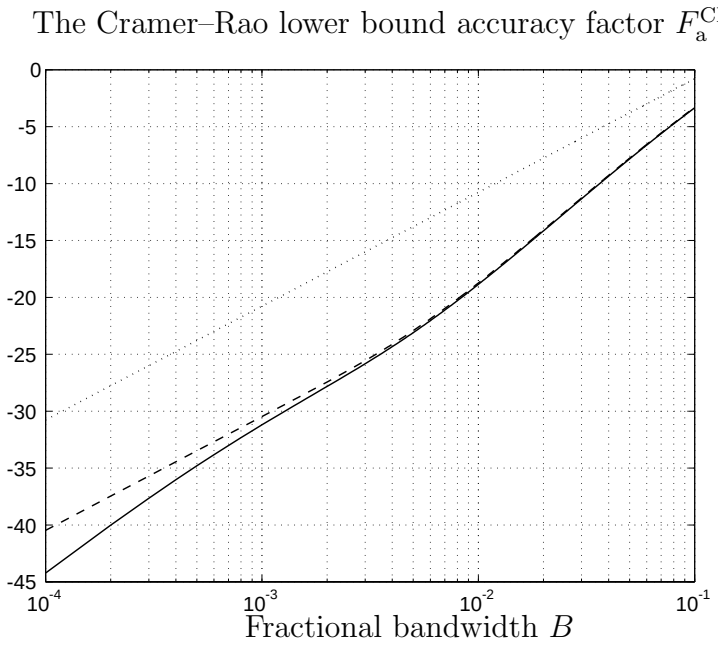


**Figure 10**: The Cramer–Rao lower bound accuracy factor $F_{\mathrm{a}}^{\mathrm{CRLB}}$ for the first 3 mode orders $n = 1, 2, 3$ as a function of fractional bandwidth $B$. Here $\theta = \pi/2$ and $ka = \frac{1}{2}$. Solid line: Three mode orders included $n = 1, 2, 3$. Dashed line: Two mode orders included $n = 1, 2$. Dotted line: One mode order included $n = 1$.

of the system. Using the properties of spherical vector modes we have modeled, quantified and illustrated how the fundamental difficulty of matching a high Q or a high bandwidth system implies a deterioration of the estimation performance when the electrical size decreases (Q increases) or when the system bandwidth increases. Hence, for a given electrical size and bandwidth, there is always a fundamental limit on the number of modes that can be effectively matched to the feeding networks and contribute to the received power, spatial diversity and estimation performance.

# Acknowledgments

The financial support by the Swedish research council is gratefully acknowledged. The authors would like to express their gratitude to Prof. George Papanicolaou for the opportunity to visit his group at the Mathematics Department, Standford University, during Mars 2003, and the many fruitful discussions on wave propagation and statistical signal processing from which the present paper has emanated.

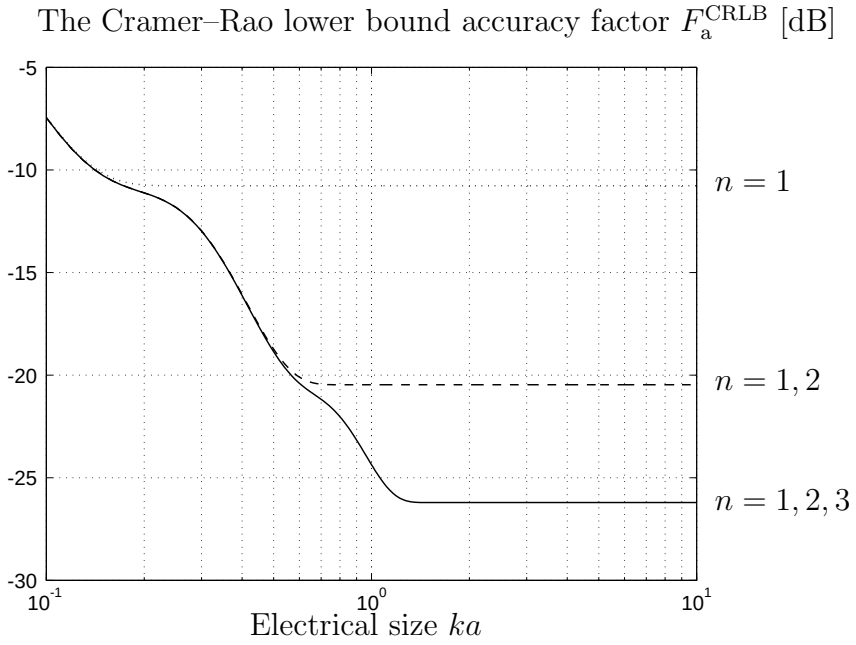


**Figure 11**: The Cramer–Rao lower bound accuracy factor $F_{\mathrm{a}}^{\mathrm{CRLB}}$ for the first 3 mode orders $n = 1, 2, 3$ as a function of electrical size $ka$. Here $\theta = \pi/2$ and $B = 0.01$. Solid line: Three mode orders included $n = 1, 2, 3$. Dashed line: Two mode orders included $n = 1, 2$. Dotted line: One mode order included $n = 1$.

# Appendix A Spherical vector mode representation and equivalent circuits

The outgoing spherical vector waves are given by

$$\boldsymbol{u}_{1ml}(k\boldsymbol{r}) = \mathrm{h}_l(x)\boldsymbol{A}_{1ml}(\hat{\boldsymbol{r}}) \tag{A.1}$$

$$\boldsymbol{u}_{2ml}(k\boldsymbol{r}) = \frac{(x\mathrm{h}_l(x))'}{x}\boldsymbol{A}_{2ml}(\hat{\boldsymbol{r}}) + \sqrt{l(l+1)}\frac{\mathrm{h}_l(x)}{x}\boldsymbol{A}_{3ml}(\hat{\boldsymbol{r}}) \tag{A.2}$$

where $x = kr$ and $\mathrm{h}_l(x)$ are the spherical Hankel functions of the second kind, the prime $(\cdot)'$ denotes differentiation with respect to $x$, and $\boldsymbol{r} = r\hat{\boldsymbol{r}}$ where $\hat{\boldsymbol{r}}$ is the unit direction vector. Further, $\boldsymbol{A}_{\tau ml}(\hat{\boldsymbol{r}})$ are the spherical vector harmonics given by

$$\boldsymbol{A}_{1ml}(\hat{\boldsymbol{r}}) = \frac{1}{\sqrt{l(l+1)}}\left(\hat{\boldsymbol{\theta}}\frac{1}{\sin\theta}\frac{\partial}{\partial\phi}\mathrm{Y}_{ml}(\hat{\boldsymbol{r}}) - \hat{\boldsymbol{\phi}}\frac{\partial}{\partial\theta}\mathrm{Y}_{ml}(\hat{\boldsymbol{r}})\right) \tag{A.3}$$

$$\boldsymbol{A}_{2ml}(\hat{\boldsymbol{r}}) = \frac{1}{\sqrt{l(l+1)}}\left(\hat{\boldsymbol{\theta}}\frac{\partial}{\partial\theta}\mathrm{Y}_{ml}(\hat{\boldsymbol{r}}) + \hat{\boldsymbol{\phi}}\frac{1}{\sin\theta}\frac{\partial}{\partial\phi}\mathrm{Y}_{ml}(\hat{\boldsymbol{r}})\right) \tag{A.4}$$

$$\boldsymbol{A}_{3ml}(\hat{\boldsymbol{r}}) = \hat{\boldsymbol{r}}\mathrm{Y}_{ml}(\hat{\boldsymbol{r}}) \tag{A.5}$$

where $\mathrm{Y}_{ml}(\hat{\boldsymbol{r}})$ are the scalar spherical harmonics [9] and $\theta$ and $\phi$ spherical coordinates.

The spherical Hankel functions of the second kind $\mathrm{h}_l(x)$ can be expressed as

$$\mathrm{h}_l(x) = \frac{\mathrm{i}^{l+1}}{x}\mathrm{e}^{-\mathrm{i}x}\sum_{k=0}^{l}\frac{(l+k)!}{k!(l-k)!}\frac{1}{(2\mathrm{i}x)^k} \tag{A.6}$$

so that the following initial relations

$$\frac{(x\mathrm{h}_0)'}{x} = -\mathrm{i}\mathrm{h}_0 \tag{A.7}$$

$$-\mathrm{h}_1 = -\mathrm{i}\mathrm{h}_0(1+\frac{1}{\mathrm{i}x}) \tag{A.8}$$

and the recursive relations

$$\frac{(x\mathrm{h}_l)'}{x\mathrm{i}^l} = \frac{\mathrm{h}_{l-1}}{\mathrm{i}^l}+\frac{l}{\mathrm{i}x}\frac{\mathrm{h}_l}{\mathrm{i}^{l+1}} \tag{A.9}$$

$$\frac{\mathrm{h}_{l+1}}{\mathrm{i}^{l+2}} = \frac{\mathrm{h}_{l-1}}{\mathrm{i}^l}+\frac{2l+1}{\mathrm{i}x}\frac{\mathrm{h}_l}{\mathrm{i}^{l+1}} \tag{A.10}$$

for $l = 1, 2, 3, \ldots$ may be verified.

The recursive relationships given above can be interpreted by using an electric circuit analogy as follows. There are two possible dual circuits associated with (A.7) through (A.10).

For *circuit 1* we define

$$\begin{array}{rcl} \dfrac{(x\mathrm{h}_l)'}{x\mathrm{i}^l} & = & \begin{cases} I_l & l \text{ even} \quad l = 0,2,4,\ldots \\ V_l & l \text{ odd} \quad l = 1,3,5,\ldots \end{cases} \\ \dfrac{\mathrm{h}_l}{\mathrm{i}^{l+1}} & = & \begin{cases} V_l & l \text{ even} \quad l = 0,2,4,\ldots \\ I_l & l \text{ odd} \quad l = 1,3,5,\ldots \end{cases} \end{array} \tag{A.11}$$

and the dual *circuit 2* is obtained by interchanging $V_l$ and $I_l$. By using $r = a$, $x = \omega a/c$ and the definitions in (A.11), the recursions (A.7) through (A.10) become

$$I_0 = V_0 \tag{A.12}$$

$$I_1 = I_0 + \frac{1}{\mathrm{i}\omega\frac{a}{c}}V_0 \tag{A.13}$$

$$V_l = V_{l-1} + \frac{1}{\mathrm{i}\omega\frac{a}{c}\frac{1}{l}}I_l,\ l = 1,3,5,\ldots \tag{A.14}$$

$$V_{l+1} = V_{l-1} + \frac{1}{\mathrm{i}\omega\frac{a}{c}\frac{1}{2l+1}}I_l,\ l = 1,3,5,\ldots \tag{A.15}$$

$$I_l = I_{l-1} + \frac{1}{\mathrm{i}\omega\frac{a}{c}\frac{1}{l}}V_l,\ l = 2,4,6,\ldots \tag{A.16}$$

$$I_{l+1} = I_{l-1} + \frac{1}{\mathrm{i}\omega\frac{a}{c}\frac{1}{2l+1}}V_l,\ l = 2,4,6,\ldots \tag{A.17}$$

and the corresponding *circuit 1* is depicted in Fig. 12 (upper circuit). The dual *circuit 2* is obtained by interchanging $V_l$ and $I_l$ in (A.12) through (A.17) and is depicted in Fig. 12 (lower circuit).

Using the definitions for $V_n$ and $I_n$ as given in (A.11) above we can now write

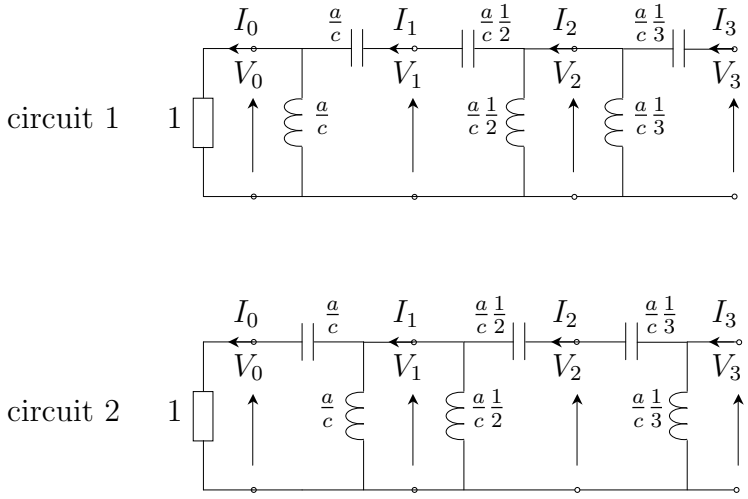


**Figure 12**: The two dual electric circuits representing spherical Hankel functions.

the TE mode ($\tau = 1$) of order $n$ in explicit form as follows

$$E_\theta = \mathrm{i}^{n+1} V_n \frac{1}{\sqrt{n(n+1)}} \frac{1}{\sin\theta} \frac{\partial}{\partial\phi} \mathrm{Y}_{mn} \tag{A.18}$$

$$-\mathrm{i}\eta H_\phi = \mathrm{i}^{n} I_n \frac{1}{\sqrt{n(n+1)}} \frac{1}{\sin\theta} \frac{\partial}{\partial\phi} \mathrm{Y}_{mn} \tag{A.19}$$

$$-E_\phi = \mathrm{i}^{n+1} V_n \frac{1}{\sqrt{n(n+1)}} \frac{\partial}{\partial\theta} \mathrm{Y}_{mn} \tag{A.20}$$

$$-\mathrm{i}\eta H_\theta = \mathrm{i}^{n} I_n \frac{1}{\sqrt{n(n+1)}} \frac{\partial}{\partial\theta} \mathrm{Y}_{mn} \tag{A.21}$$

$$-\mathrm{i}\eta H_r = \frac{\mathrm{h}_n}{ka} \sqrt{n(n+1)} \mathrm{Y}_{mn} \tag{A.22}$$

where circuit 1 is used for even order and circuit 2 for odd order.

The TM mode ($\tau = 2$) of order $n$ is given by

$$E_\theta = \mathrm{i}^{n} V_n \frac{1}{\sqrt{n(n+1)}} \frac{\partial}{\partial\theta} \mathrm{Y}_{mn} \tag{A.23}$$

$$\mathrm{i}\eta H_\phi = \mathrm{i}^{n+1} I_n \frac{1}{\sqrt{n(n+1)}} \frac{\partial}{\partial\theta} \mathrm{Y}_{mn} \tag{A.24}$$

$$E_\phi = \mathrm{i}^{n} V_n \frac{1}{\sqrt{n(n+1)}} \frac{1}{\sin\theta} \frac{\partial}{\partial\phi} \mathrm{Y}_{mn} \tag{A.25}$$

$$-\mathrm{i}\eta H_\theta = \mathrm{i}^{n+1} I_n \frac{1}{\sqrt{n(n+1)}} \frac{1}{\sin\theta} \frac{\partial}{\partial\phi} \mathrm{Y}_{mn} \tag{A.26}$$

$$E_r = \frac{\mathrm{h}_n}{ka} \sqrt{n(n+1)} \mathrm{Y}_{mn} \tag{A.27}$$

where circuit 1 is used for odd order and circuit 2 for even order.

The four circuits necessary to describe the TE and TM modes for even and odd orders are depicted in Fig. 13 below. The input impedance of the circuits are $\eta\frac{V_n}{I_n} = \frac{E_\theta}{H_\phi} = -\frac{E_\phi}{H_\theta}$ for both TE and TM modes.

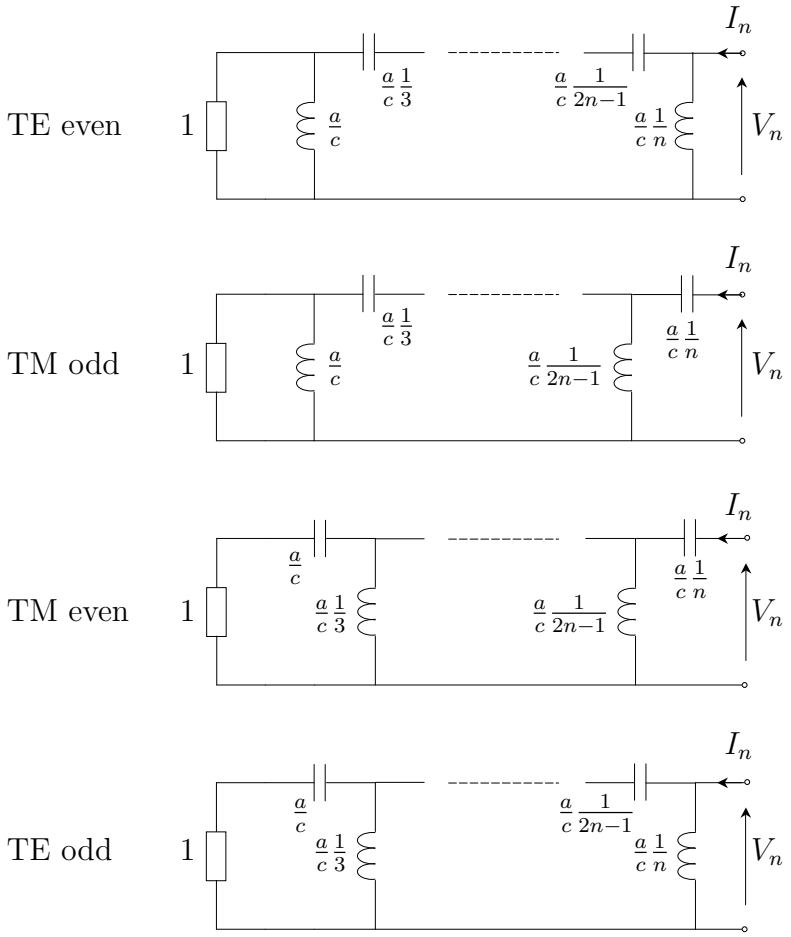


**Figure 13**: Electric circuit analogy for TE and TM modes, even and odd orders.

In the *far field* when $r \to \infty$, the spherical Hankel functions can be approximated with $\mathrm{h}_l(x) = \frac{\mathrm{i}^{l+1}}{x}\mathrm{e}^{-\mathrm{i}x} + O(x^{-2})$ and $\mathrm{h}_l'(x) = \frac{\mathrm{i}^{l}}{x}\mathrm{e}^{-\mathrm{i}x} + O(x^{-2})$. The outgoing spherical vector waves can therefore be approximated by $\boldsymbol{u}_{\tau ml}(k\boldsymbol{r}) = \mathrm{i}^{l+2-\tau}\frac{\mathrm{e}^{-\mathrm{i}kr}}{kr}\boldsymbol{A}_{\tau ml}(\hat{\boldsymbol{r}})$. Hence, the far field expression is

$$\boldsymbol{E}(\boldsymbol{r}) = \frac{\mathrm{e}^{-\mathrm{i}kr}}{kr}\boldsymbol{F}(\hat{\boldsymbol{r}}) \tag{A.28}$$

where $\boldsymbol{F}(\hat{\boldsymbol{r}})$ is the *far field amplitude* given by

$$\boldsymbol{F}(\hat{\boldsymbol{r}}) = \sum_{l=1}^{\infty}\sum_{m=-l}^{l}\sum_{\tau=1}^{2}\mathrm{i}^{l+2-\tau}f_{\tau ml}\boldsymbol{A}_{\tau ml}(\hat{\boldsymbol{r}}). \tag{A.29}$$

The total power $P_s$ transmitted by the antenna is given by

$$P_s = \frac{1}{2\eta k^2}\int_\Omega |\boldsymbol{F}(\hat{\boldsymbol{r}})|^2\,\mathrm{d}\Omega = \frac{1}{2\eta k^2}\sum_{l=1}^{\infty}\sum_{m=-l}^{l}\sum_{\tau=1}^{2}|f_{\tau ml}|^2 \tag{A.30}$$

where $\Omega$ denotes the unit sphere and $d\Omega$ the differential solid angle, cf. [9].

# References


[1] A. Boström, G. Kristensson, and S. Ström. Transformation properties of plane, spherical and cylindrical scalar and vector wave functions. In V. V. Varadan, A. Lakhtakia, and V. K. Varadan, editors, *Field Representations and Introduction to Scattering*, Acoustic, Electromagnetic and Elastic Wave Scattering, chapter 4, pages 165–210. Elsevier Science Publishers, Amsterdam, 1991.

[2] L. J. Chu. Physical limitations of Omni-Directional antennas. *Appl. Phys.*, **19**, 1163–1175, 1948.

[3] R. E. Collin and S. Rothschild. Evaluation of antenna Q. *IEEE Trans. Antennas Propagat.*, **12**, 23–27, January 1964.

[4] S. Drabowitch, A. Papiernik, H. Griffiths, J. Encinas, and B. L. Smith. *Modern Antennas*. Chapman & Hall, 1998.

[5] R. M. Fano. Theoretical limitations on the broadband matching of arbitrary impedances. *Journal of the Franklin Institute*, **249**(1,2), 57–83 and 139–154, 1950.

[6] R. L. Fante. Quality factor of general antennas. *IEEE Trans. Antennas Propagat.*, **17**(2), 151–155, March 1969.

[7] W. Geyi, P. Jarmuszewski, and Y. Qi. The Foster reactance theorem for antennas and radiation Q. *IEEE Trans. Antennas Propagat.*, **48**(3), 401–408, March 2000.

[8] R. C. Hansen. Fundamental limitations in antennas. *Proc. IEEE*, **69**(2), 170–182, 1981.

[9] R. F. Harrington. *Time Harmonic Electromagnetic Fields*. McGraw-Hill, New York, 1961.

[10] K.-C. Ho, K.-C. Tan, and B. T. G. Tan. Linear dependence of steering vectors associated with tripole arrays. *IEEE Trans. Antennas Propagat.*, **46**(11), 1705–1711, November 1998.

[11] S. M. Kay. *Fundamentals of Statistical Signal Processing, Estimation Theory*. Prentice-Hall, Inc., NJ, 1993.

[12] H. Krim and M. Viberg. Two decades of array signal processing research: the parametric approach. *IEEE Signal Processing Magazine*, **13**(4), 67–94, July 1996.

[13] G. Kristensson. *Spridningsteori med antenntillämpningar*. Studentlitteratur, Lund, 1999. (In Swedish).

[14] J. Li. Direction and polarization estimation using arrays with small loops and short dipoles. *IEEE Trans. Antennas Propagat.*, **41**(3), 379–387, March 1993.

[15] J. Li and P. Stoica. Efficient parameter estimation of partially polarized electromagnetic waves. **42**(11), 3114–3125, November 1994.

[16] J. S. McLean. A re-examination of the fundamental limits on the radiation $Q$ of electrically small antennas. *IEEE Trans. Antennas Propagat.*, **44**(5), 672–676, May 1996.

[17] K. S. Miller. *Complex Stochastic Processes.* Addison–Wesley Publishing Company, Inc., 1974.

[18] P. Stoica and A. Nehorai. MUSIC, maximum likelihood, and Cramer-Rao bound: further results and comparisons. **38**(12), 2140–2150, December 1990.

[19] A. Swindlehurst and M. Viberg. Subspace fitting with diversely polarized antenna arrays. *IEEE Trans. Antennas Propagat.*, **41**(12), 1687–1694, December 1993.

[20] H. L. Thal. Exact circuit analysis of spherical waves. *IEEE Trans. Antennas Propagat.*, **26**(2), 282–287, March 1978.

[21] H. L. V. Trees. *Optimum Array Processing.* John Wiley & Sons, Inc., New York, 2002.

[22] M. Viberg, P. Stoica, and B. Ottersten. Maximum likelihood array processing in spatially correlated noise fields using parameterized signals. **45**(4), 996–1004, April 1997.

[23] A. J. Weiss and B. Friedlander. Maximum likelihood signal estimation for polarization sensitive arrays. *IEEE Trans. Antennas Propagat.*, **41**(7), 918–925, July 1993.

[24] K. T. Wong and M. D. Zoltowski. Closed–form direction finding and polarization estimation with arbitrarily spaced electromagnetic vector–sensors at unknown locations. *IEEE Trans. Antennas Propagat.*, **48**(5), 671–681, May 2000.